



CoMamba: Real-time Cooperative Perception Unlocked with State Space Models

Jinlong Li¹, Xinyu Liu², Baolu Li², Runsheng Xu³, Jiachen Li⁴, Hongkai Yu², Zhengzhong Tu¹

Abstract—Cooperative perception systems play a vital role in enhancing the safety and efficiency of vehicular autonomy. Although recent studies have highlighted the efficacy of vehicle-to-everything (V2X) communication techniques in autonomous driving, a significant challenge persists: how to efficiently integrate multiple high-bandwidth features across an expanding network of connected agents such as vehicles and infrastructure. In this paper, we introduce CoMamba, a novel cooperative 3D detection framework designed to leverage state-space models for real-time onboard vehicle perception. Compared to prior state-of-the-art transformer-based models, CoMamba enjoys being a more scalable 3D model using bidirectional state space models, bypassing the quadratic complexity pain-point of attention mechanisms. Through extensive experimentation on V2X/V2V datasets, CoMamba achieves superior performance compared to existing methods while maintaining real-time processing capabilities. The proposed framework not only enhances object detection accuracy but also significantly reduces processing time, making it a promising solution for next-generation cooperative perception systems in intelligent transportation networks.

I. INTRODUCTION

Recently, the new paradigm of cooperative perception [1]–[3] that engages multiple connected and automated Vehicles (CAVs) has captivated massive research interest. By leveraging vehicle-to-everything (V2X) or vehicle-to-vehicle (V2V) communication, intelligent actors are now capable of “talking” to their nearby neighbors to share information like pose and sensory data (e.g., point clouds, RGB images, or neural features). Although V2X cooperative systems have immense potential to transform the transportation industry, designing efficient fusion strategies to effectively incorporate large, high-dimensional features remains a challenging and unsolved research topic. Motivated by the phenomenal study on Vision Transformer [4], which has demonstrated strong visual learning capabilities on generic vision tasks, prior V2X perception models have been investigating the use of Transformers as the foundational architecture for cooperative perception [2], [5]–[7]. For example, OPV2V [1] implements a single-head self-attention module to fuse features for V2V perception. V2X-ViT [5] presents a unified Vision Transformer (ViT) architecture for V2X perception, capable of capturing the heterogeneous nature of V2X systems. CoBEVT [2] proposes a holistic vision Transformer for multi-view cooperative semantic segmentation. These methods enhance their visual learning capability by leveraging

self-attention mechanisms to model long-range spatial interactions. However, the practical deployment of these methods in large-scale, complex real-world scenarios remains limited due to the slow inference time and worse scalability imbued in attention-based architectures.

To overcome these limitations, recent advances in State Space Models (SSMs) [8]–[10] offer competitive alternatives to the notoriously compute-intensive Transformers. A notable model, Mamba [11], capably attains long-sequence modeling with a significantly lower *linear complexity* by maintaining a continuous, linear update path through state space. This efficient design demonstrates impressive performances in long sequence modeling tasks in natural language processing [12]–[14]. Motivated by this success, recent studies have explored its potential for fundamental vision tasks [15]–[18], showcasing impressive performance while considerably fewer computational resources compared to Transformers. However, while most of these studies predominantly focus on 2D vision tasks such as image recognition, the potential of SSMs to serve as a generic backbone for more challenging vision tasks remains unexplored, particularly in areas involving higher-order visual interaction modeling, such as 3D sequence modeling and space-time interactions.

In this paper, we explore the potential adoption of state-space models for the challenging V2X/V2V cooperative perception task, which involves high-order, multimodal visual information fusion using LiDAR scans. We present CoMamba, a generic Mamba-based architecture for efficient V2X cooperative perception that perfectly balances detection performance and computational efficiency. As illustrated in Fig. 1 our CoMamba fusion network comprises two key modules: the Cooperative 2D-Selective-Scan Module and the Global-wise Pooling Module, which we specifically tailored for conducting feature fusion using an intermediate fusion-based cooperative framework. Together, these modules empower CoMamba to achieve state-of-the-art perception performance on public V2X/V2V perception datasets [1], [5], [19], with significant speed-up as compared to previous transformer-based methods. Notably, CoMamba unlocks *real-time* cooperative perception with a low latency of 37.1 ms per communication, which translates to 26.9 FPS inference speed with merely a 0.64 GB GPU memory footprint, 19.4% faster than prior state-of-the-art¹. Our contributions can be summarized as: leftmargin=*

¹Texas A&M University, TACO-Group. ²Cleveland State University, Cleveland Vision & AI Lab. ³University of California, Los Angeles. ⁴University of California, Riverside.

*Corresponding Author: tzz@tamu.edu

¹Benchmarked on a single 48GB NVIDIA RTX A6000 card.

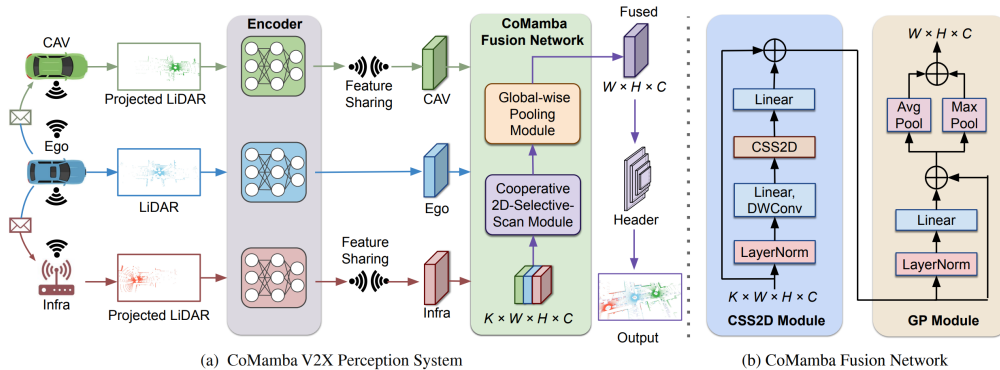


Fig. 1: **Overview of our CoMamba V2X-based perception framework.** (a) CoMamba V2X perception system involves V2X metadata sharing, LiDAR visual encoder, feature sharing, and CoMamba fusion network to conduct final prediction. (b) our CoMamba fusion network leverages the Cooperative 2D-Selective-Scan Module to effectively fuse the complex interactions present in high-resource-cost V2X data sequences. The Global-wise Pooling Module efficiently attains global information among the overlapping features of the CAVs.

- We propose CoMamba, the first attempt to explore the potential of linear-complexity Mamba models for V2X cooperative perception. Our CoMamba is a novel V2X perception framework that efficiently models V2X feature interactions using state-space models. Notably, CoMamba scales linearly with the increasing number of connected agents (as explained in Fig. 3), whereas previous transformer models all suffer from quadratic complexity with respect to total data dimensionality.
- We design two modules inside the CoMamba framework: the Cooperative 2D-Selective-Scan Module for highly efficient 3D spatial interactions and the Global-wise Pooling Module for information aggregation to conduct point cloud-based 3D object detection.
- Our comprehensive experimental results on both simulated and real-world datasets have demonstrated that CoMamba exceeds the previous state-of-the-art cooperative detection models while at a significantly lower computational cost. Our ablation studies have shown the efficacy of each component design in contributing to the overall performance.

II. RELATED WORK

V2X cooperative perception. V2X systems can substantially enhance the perception capabilities of autonomous vehicles by enabling data sharing among CAVs. This cooperative perception strategy significantly extends the detection range beyond immediate surroundings, thereby improving driving safety in complex scenarios [20]–[23]. In terms of modeling, V2X-ViT [5] introduces a unified transformer framework specifically designed to handle the heterogeneous and multi-scale nature of multi-scale V2X systems. Where2comm [24] presents a multi-agent perception framework guided by spatial confidence maps to effectively balance communication bandwidth and perception performance. CoBEVT [2] employs an axial-attention-based multi-agent perception framework that collaboratively generates predictions from sparse locations to capture long-range dependencies. Additionally, SCOPE [25] integrates temporal context into a learning-based framework for multi-agent perception to boost the capabilities of the ego agent. **Deployment of**

V2X perception system. Despite the great potential of V2X/V2V systems, deploying these architectures in real-world scenarios requires overcoming numerous fundamental challenges. These include model heterogeneity [26], [27], lossy communication [28], [29], adversarial vulnerability [30], [31], location errors [32], and communication latency [5], [33], to name a few. Among these, V2X-ViT [5] introduces a delay-aware positional encoding module to mitigate communication delays and GPS localization errors using a unified Vision Transformer. FDA [34] addresses the distribution gap among various private data through a cross-domain learning approach with a feature distribution-aware aggregation framework. S2R-ViT [35] introduces a sim-to-real transfer learning method to reduce the deployment gap affecting V2V perception.

State space models State space models (SSMs) [8]–[10], inspired by linear time-invariant (LTI) systems, emerged as an efficient alternative to transformers for sequence-to-sequence modeling tasks. One phenomenal model, Mamba [11], introduces a selection mechanism for dynamically extracting features from sequence data to capture long-range contextual dependencies. Mamba outperforms Transformers on various 1D datasets while requiring significantly fewer computational resources. Motivated by its success in language modeling, state space models have also been extended to various computer vision tasks [15]–[18]. For example, the Visual State-Space Model (Vim) [36] integrated SSM with bidirectional scanning, enhancing the relational mapping between image patches. VMamba [37] further introduces a cross-scan technique, a four-directional modeling approach that uncovers additional spatial connections to fully capture interrelations among image patches. However, it remains unknown whether SSMs can serve as a new foundation model for more generic vision tasks, such as 3D point cloud understanding, 3D vision, and autonomous driving.

III. METHODOLOGY

Current ViT-based V2X perception systems suffer from the quadratic complexity of attention mechanisms as well as large memory footprints, making them impractical for deployment in large-scale, complex real-world scenarios.

Despite some efforts being made to introduce sparse attention for efficiency [2], [5], these models fail to scale favorably as the number of agents (or total gathered feature dimensionality in ego vehicle) grows larger. We are making the first attempt to explore the potential of linear-complexity Mamba models in the context of V2X cooperative perception to overcome the scalability limitations. Inspired by the impressive efficiency and modeling capabilities of SSMs, we build an entirely attention-free architecture, dubbed the CoMamba V2X-based perception framework (illustrated in (a) of Fig. 1), that is purely based on SSMs. Our CoMamba model comprises two major components: the Cooperative 2D-Selective-Scan module and the Global-wise Pooling module. Thanks to the efficiency-friendly designs in SSMs, our CoMamba model achieves **real-time inference speed** (26.9 FPS), and scales remarkably better than prior state-of-the-art transformer models. In this section, we will detail the architectural design of our proposed CoMamba model.

A. Preliminaries

State space models. State space models (SSMs) [8], [10], [38] are continuous sequence-to-sequence modeling systems known for their linear time-invariant (LTI) properties. They map a 1D input sequence $I(x) \in \mathbb{R}$ to a 1D output sequence $O(x) \in \mathbb{R}$ through an intermediate hidden state $h(x) \in \mathbb{R}^N$, as illustrated below:

$$h'(x) = \mathbf{A}h(x) + \mathbf{B}I(x), y(x) = \mathbf{C}h(x), \quad (1)$$

where $\mathbf{A} \in \mathbb{R}^{N \times N}$, $\mathbf{B} \in \mathbb{R}^{N \times 1}$, and $\mathbf{C} \in \mathbb{R}^{1 \times N}$ are the evolution and projection parameters, respectively. SSMs effectively capture global system awareness through an implicit mapping to latent states. When \mathbf{A} , \mathbf{B} , and \mathbf{C} have constant values, Eq. 1 defines an LTI system in [8]. Otherwise, Mamba introduces a linear time-varying (LTV) system [11]. LTI systems inherently lack the ability to perceive content, whereas LTV systems are designed to be input-aware, an important property that attention models also enjoy. This crucial distinction allows Mamba to surpass the limitations of SSMs, allowing for even stronger modeling capabilities.

To facilitate discretization for deployment in deep learning, a timescale parameter, denoted as $\Delta \in \mathbb{R}$, is introduced to transform the continuous parameters \mathbf{A} and \mathbf{B} into their discrete counterparts, represented as $\bar{\mathbf{A}}$ and $\bar{\mathbf{B}}$. Using the zero-order hold as the transformation algorithm, the discrete parameters are formulated as follows:

$$\bar{\mathbf{A}} = \exp(\Delta \mathbf{A}), \bar{\mathbf{B}} = (\Delta \mathbf{A})^{-1}(\exp(\Delta \mathbf{A}) - \mathbf{I}) \cdot \Delta \mathbf{B}. \quad (2)$$

The discrete form of Eq. 1 can then be expressed as:

$$h_x = \bar{\mathbf{A}}h_{x-1} + \bar{\mathbf{B}}I_x, y_x = \mathbf{C}h_x. \quad (3)$$

Selective scan mechanism. Traditional SSMs face limitations due to their LTI properties, resulting in invariant parameters irrespective of variations in the input. To overcome this limitation, the Selective State Space Model (Mamba) [11] incorporates a selective scan mechanism that integrates three classical techniques: kernel fusion, parallel scan, and recomputation. By employing the selective scan

algorithm, Mamba achieves strong modeling capacity while enjoying efficient computational complexity and reduced memory requirements, which contribute to its fast inference.

B. CoMamba V2X-based Perception System Design

The system design of the CoMamba V2X-based perception framework pipeline is illustrated in (a) of Fig. 1. First, we select an ego vehicle from the CAVs to construct a spatial graph that includes nearby CAVs within the V2X communication sphere. Recognizing the analogous data-sharing capabilities between CAVs and intelligent infrastructures, our methodology equates each infrastructure unit to a CAV. Then, adjacent CAVs capture and project their raw LiDAR data onto the ego vehicle's coordinate frame using both their own and the ego vehicle's GPS positions. The point clouds from the ego vehicle and other CAVs are represented as $\mathbf{P}_{ego} \in \mathbb{R}^{4 \times s}$ and $\mathbf{P}_{cav} \in \mathbb{R}^{4 \times s}$, respectively. In the V2X perception system, each CAV has its own encoder for extracting LiDAR features. After feature extraction, the ego vehicle receives visual features from neighboring CAVs via V2X communication. The intermediate features collected from N surrounding CAVs are denoted as $\mathbf{F}_{cav} \in \mathbb{R}^{N \times H \times W \times C}$, while those of the ego vehicle are denoted as $\mathbf{F}_{ego} \in \mathbb{R}^{1 \times H \times W \times C}$. \mathbf{F}_{ego} , along with those \mathbf{F}_{cav} received from other CAVs, are processed by our CoMamba fusion network. The resulting feature map is then passed to a prediction module for 3D bounding-box regression and classification. Our CoMamba cooperative perception system $\Gamma(\cdot)$ for LiDAR-based 3D object detection can be formulated as follows:

$$\Gamma(\mathbf{P}_{cav}, \mathbf{P}_{ego}) = \Phi(\mathbf{CoMamba}(\mathbf{F}_{cav}, \mathbf{F}_{ego})), \quad (4)$$

$$\mathbf{F}_{cav} = \mathbf{E}_{cav}(\mathbf{P}_{cav}), \mathbf{F}_{ego} = \mathbf{E}_{ego}(\mathbf{P}_{ego}), \quad (5)$$

where $\mathbf{CoMamba}(\cdot)$ is our proposed CoMamba fusion network, which is responsible for efficiently fusing the shared features. $\Phi(\cdot)$ is the prediction header for 3D object detection. \mathbf{E}_{ego} and \mathbf{E}_{cav} refer to the feature encoders of the ego vehicle and other CAVs, respectively.

C. CoMamba Fusion Network

Overall architecture. The schematic block diagram of the CoMamba fusion network is illustrated in Fig. 1(b). After encoding by \mathbf{E}_{ego} and \mathbf{E}_{cav} , we obtain intermediate neural features \mathbf{F}_{ego} and \mathbf{F}_{cav} from the ego vehicle and other CAVs, respectively. These features are then fed into the Cooperative 2D-Selective-Scan (CSS2D) module to conduct linear-time 3D information mixing. In the CSS2D module, We first normalize them by applying Layer Normalization (LN), then followed by a feature extraction using the 3×3 depth-wise convolution and Linear layers to obtain their feature maps. The processed features are fed into the CSS2D process as shown in Fig. 2 to vision data without compromising its advantages. Then the following features are fed into LN again and the Linear layer with skip-connections, and MaxPool and AvgPool operation modules, which form our Global-wise Pooling Module (GPM) to obtain the final fused feature $\mathbf{F}_{fused} \in \mathbb{R}^{H \times W \times C}$.

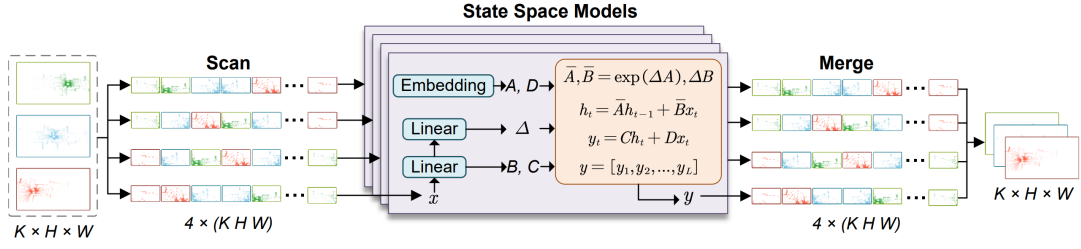


Fig. 2: **Illustration of the Cooperative 2D-Selective-Scan (CSS2D) process.** The features of K CAVs, represented as $\mathbb{R}^{H \times W}$, are embedded into patches. These patches are then traversed along four different scanning paths, with each 1D sequence (KHW) independently processed by distinct Mamba blocks [11] in parallel. Afterward, the resulting outputs are reshaped and merged to form the 3D feature maps, which maintain the same dimensions as the input features. In this instance, we use $K = 3$ as an illustrative example.

Cooperative 2D-Selective-Scan (CSS2D). We utilize the four-directional sequence modeling approach proposed in [37] to improve global spatial awareness of high-order spatial features. Specifically, the input feature maps \mathbf{F}_{ego} and \mathbf{F}_{cav} are first flattened into dimensions of $\mathbb{R}^{KHW \times C}$, where $K = N + 1$. This process ensures that all CAVs' neural features within the V2X communication range are flattened into 1D sequence sets S_K . These 1D sequences are then individually processed through Mamba blocks [11] for feature extraction to obtain the enhanced 1D sequences \bar{S}_K . Then we unflatten the outputs \bar{S}_K and combine them to obtain the interactive feature maps $\hat{\mathbf{F}}_{(ego,cav)} \in \mathbb{R}^{K \times H \times W \times C}$. The overview of CSS2D process $\text{CSS2D}(\cdot)$ is formulated as

$$\text{CSS2D}(\mathbf{F}_{cav}, \mathbf{F}_{cav}) = \text{Merge}(\text{SSM}(\text{Scan}(\mathbf{F}_{ego}, \mathbf{F}_{cav}))). \quad (6)$$

where $\text{SSM}(\cdot)$ is the selective scan mechanism [11]. $\text{Scan}(\cdot)$, and $\text{Merge}(\cdot)$ represent the operation of flattening, and unflattening, respectively.

Global-wise Pooling Module (GPM). After being processed by the CSS2D module, the enhanced features are denoted as $\hat{\mathbf{F}}_{(ego,cav)}$. To attain global-aware properties among all these CAVs' overlapping features, we utilize the spatial features generated by max pooling and average pooling, which is shown in Fig. 1(b). The $\hat{\mathbf{F}}_{(ego,cav)} \in \mathbb{R}^{K \times H \times W \times C}$ features are first fed into the Layer Norm and Linear layer (LLs), then reduced to $\hat{\mathbf{F}}_{(ego,cav)}^{max} \in \mathbb{R}^{1 \times H \times W \times C}$ and $\hat{\mathbf{F}}_{(ego,cav)}^{avg} \in \mathbb{R}^{1 \times H \times W \times C}$ by calculating max pooling and average pooling along the first channel axis. These two feature maps are combined to get the final fused feature $\hat{\mathbf{F}}_{fused} \in \mathbb{R}^{1 \times H \times W \times C}$ which contains two kinds of global spatial information from the original intermediate feature maps. This process can be formulated as

$$\text{GPM}(\hat{\mathbf{F}}_{(ego,cav)}) = \text{P}_{\max}(\text{LLs}(\hat{\mathbf{F}}_{(ego,cav)})) + \quad (7)$$

$$\text{P}_{\text{ave}}(\text{LLs}(\hat{\mathbf{F}}_{(ego,cav)})), \quad (8)$$

where $\text{GPM}(\cdot)$ denotes our proposed Global-wise Pooling Module. $\text{P}_{\max}(\cdot)$, and $\text{P}_{\text{ave}}(\cdot)$ represent the operation of max pooling and average pooling along the first channel axis, respectively. For 3D object detection, we use the smooth L1 loss for bounding box regression and focal loss [39] for classification, which constructs our final loss for training.

Complexity analysis. Current V2X methods are predominantly based on Transformer architectures [2], [5]. They have made considerable efforts to optimize spatial computational

efficiency but have largely overlooked the potential increased number of connected agents. With the future proliferation of intelligent agents and V2X perception systems, the scale of agents required for cooperative perception in V2X systems will inevitably grow exponentially. However, prior cooperative transformers will struggle to handle more CAVs due to self-attention models' quadratic complexity and memory footprint. We would like to highlight that our proposed CoMamba is truly scalable in terms of the entire spatial dimension, including both 2D feature dimensions and the number of agents. Fig. 3 demonstrates the FLOPs, latency, and memory footprint comparisons of our CoMamba against prior state-of-the-art transformer models, V2X-ViT [5] and CoBEVT [2]. We may see that both Transformer models suffer from quadratic complexity in both metrics, while CoMamba enjoys being linear. When the number of agents exceeds 20, the memory capacity of a single 48GB GPU device (NVIDIA RTX A6000 card) cannot suffice to run the other two models anymore. In contrast, CoMamba leverages the advantages of SSMs to attain linear costs in GFLOPs, latency, and GPU memory relative to the number of agents, while maintaining excellent performance (Sec. IV-B).

IV. EXPERIMENT

A. Datasets and experimental setup

Dataset. We conducted extensive experiments on three multi-agent datasets: OPV2V [1], V2XSet [5], and V2V4Real [19]. OPV2V [1] and V2XSet [5] are simulated datasets generated using the CARLA simulator and the OpenCDA co-simulation framework [40]. The OPV2V dataset is organized into 6,764 frames for training, 1,981 frames for validation, and 2,719 frames for testing. Of these, 2,170 frames from CARLA Towns and 594 frames from Culver City are used as two distinct OPV2V testing sets. V2XSet is structured into training, validation, and testing segments, with 6,694, 1,920, and 2,833 frames respectively. V2V4Real [19] is an extensive real-world V2V perception dataset, collected by two CAVs in Columbus, OH, USA. It contains 20,000 LiDAR frames covering intersections, highway ramps, and urban roads. It is split into 14,210/2,000/3,986 frames for training/validation/testing, respectively.

Compared methods. Here, seven state-of-the-art V2X fusion methods are evaluated, all of which employ *Intermediate Fusion* as the primary strategy: AttFuse [1], V2VNet [41], F-Cooper [3], V2X-ViT [5], CoBEVT [2], Where2Comm [24],

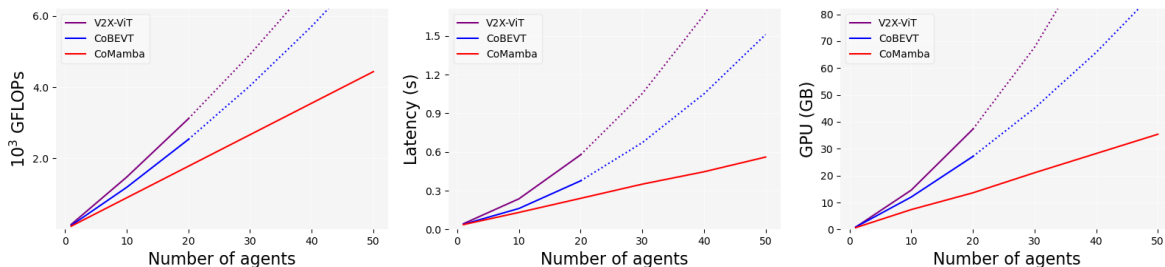


Fig. 3: **Scalability comparisons:** CoMamba, V2X-ViT [5] and CoBEVT [2] in GFLOPs, latency, and GPU memory footprint with respect to the number of agents (total feature dimensions). The dotted lines indicate the estimated values when tested GPUs are out-of-memory.

TABLE I: **LiDAR-based 3D detection performance comparison.** We show Average Precision (AP) at IoU=0.5 and 0.7 on four V2X testing sets from OPV2V, V2X-Set, and V2V4Real datasets.

Method	OPV2V Default [1]		OPV2V Culver City [1]		V2XSet [5]		V2V4Real [19]	
	AP@0.5	AP@0.7	AP@0.5	AP@0.7	AP@0.5	AP@0.7	AP@0.5	AP@0.7
No Fusion	67.9	60.2	55.7	47.1	60.6	40.2	39.8	22.0
F-Cooper [3]	86.3	75.9	81.5	71.9	84.0	68.0	53.6	26.7
AttFuse [1]	85.1	73.5	83.8	70.0	80.7	66.4	57.7	27.5
V2VAM [28]	85.7	74.3	84.1	70.9	81.3	66.1	56.8	28.1
V2VNet [41]	88.1	82.2	86.8	73.4	84.5	67.7	56.4	28.5
Where2Comm [24]	89.7	80.6	84.5	65.8	85.5	72.1	58.2	28.3
V2X-ViT [5]	87.3	72.6	87.1	72.0	88.2	71.2	55.9	29.3
CoBEVT [2]	90.8	82.1	86.6	74.8	84.1	71.5	58.6	29.7
CoMamba (ours)	91.9	83.3	87.4	75.2	88.3	72.9	63.9	35.5

TABLE II: **Camera-only 3D detection performance comparison.** We show Average Precision (AP) at IoU=0.5 and 0.7 on the OPV2V and V2XSet datasets.

Method	OPV2V Default [1]		V2XSet [5]	
	AP@0.5	AP@0.7	AP@0.5	AP@0.7
No Fusion	45.94	25.56	30.37	13.79
Late Fusion	77.62	51.92	51.41	25.59
V2VNet	79.06	57.59	59.54	39.00
Where2Comm	77.14	58.60	61.69	43.96
V2X-ViT	78.41	58.38	59.14	41.23
CoBEVT	80.26	59.34	58.84	40.81
CoAlign	80.21	60.46	64.79	39.64
CoMamba(ours)	83.12	63.23	69.16	46.58

and V2VAM [28]. We train all these methods on three cooperative perception training sets (*i.e.* OPV2V, V2XSet, and V2V4Real) for a fair comparison. Then, these methods are evaluated using their testing sets to assess their performance.

Evaluation metrics. The final 3D vehicle detection accuracy is selected as our performance evaluation. Following [1], [5], we set the evaluation range as $x \in [-140, 140]$ meters, $y \in [-40, 40]$ meters, where all the CAVs are included in this spatial range in the experiment. We measure the accuracy with Average Precisions (AP) at Intersection-over-Union (IoU) thresholds of 0.5 and 0.7.

Experiment settings. To ensure a fair comparison, all methods employ PointPillar [42] as the point cloud encoder. We use the Adam optimizer [43] with an initial learning rate of 10^{-3} , which is gradually decayed every 10 epochs by a factor of 0.1. Following the setup in [5], all models are trained on two NVIDIA RTX A6000 GPU cards. We also conducted extensive experiments on the camera-only cooperative perception task. We utilize the single-scale, history-free BEVFormer as the 3D object detector for individual agents. We employ EfficientNet as the image backbone and use a finer grid resolution of 0.4 meters to preserve detailed spatial information.

B. Quantitative Evaluation

Results on simulation data. As shown in Table I, all CP methods significantly surpass the *NO Fusion*, demonstrating the benefits of the V2X perception system on three simulated testing sets. In the OPV2V Default testing set, our proposed CoMamba outperforms the other seven advanced fusion methods, achieving 91.9%/83.3% for AP@0.5/0.7, highlighted in bold in Table I. In the V2XSet testing set, V2X-ViT [5] achieves 88.2%/71.2% for AP@0.5/0.7, while our CoMamba attains 88.3%/72.9% for AP@0.5/0.7, surpassing

V2X-ViT [5] with an AP@0.7 improvement of 1.7%. These results indicate that our proposed CoMamba can efficiently enhance the interaction between CAVs' features, achieving the best performance in simulated V2X point cloud data.

Results on real-world data. The simulated point cloud data does not accurately reflect the challenges encountered in real-world deployment, as shown in Fig. 4. To address this, we evaluate all fusion methods on the real-world V2V4Real testing set, presented in Table I. Our proposed CoMamba outperforms the other seven advanced fusion methods, achieving 63.9%/35.5% for AP@0.5/0.7, which is higher than the second-best fusion method, CoBEVT [2], with an AP@0.5/0.7 improvement of 5.3%/5.8%. This indicates that our CoMamba, with its CSS2D and GPM modules, can effectively enhance global interaction capabilities in complex real-world V2X data, resulting in excellent cooperative perception performance.

Results on visual 3D object detection. As shown in Table II, our proposed CoMamba model surpasses other advanced fusion methods, delivering superior 3D perception performance on the camera-only V2X perception system.

TABLE III: **Component ablation study.**

	V2XSet [5]		V2V4Real [19]	
	AP@0.5	AP@0.7	AP@0.5	AP@0.7
Baseline	71.4	54.7	48.5	24.1
w/ CSS2D	86.9	71.5	58.1	33.9
w/ GPM	84.4	68.4	57.3	30.5
CoMamba	88.3	72.9	63.9	35.5

Efficiency analysis. Fig. 3 illustrates the processing performance comparison with current popular V2X perception methods. In current V2X datasets, our CoMamba achieves real-time perception performance with an inference speed of *26.9 FPS while utilizing only 0.64 GB of GPU memory.*

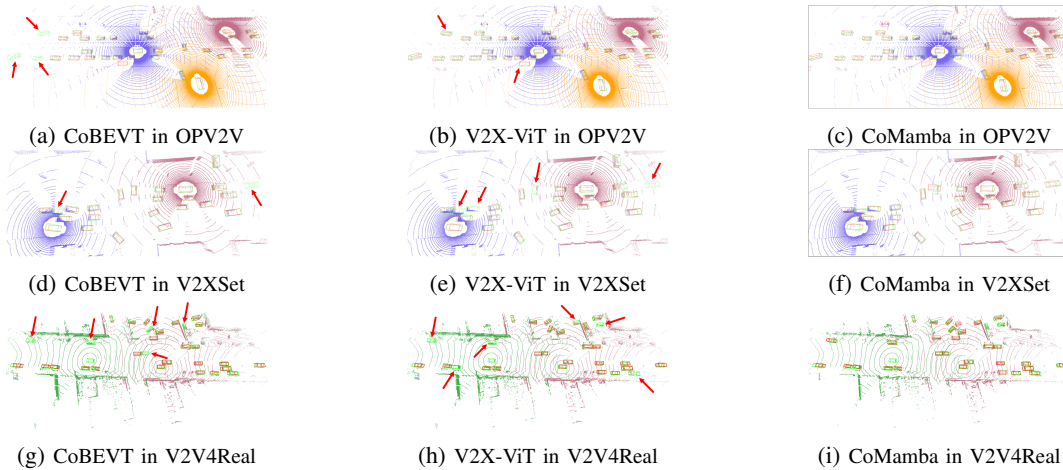


Fig. 4: **Visualizations of 3D object detection results.** Green and red 3D bounding boxes represent the ground truth and prediction, respectively. Some false detection examples are highlighted using the red arrow.

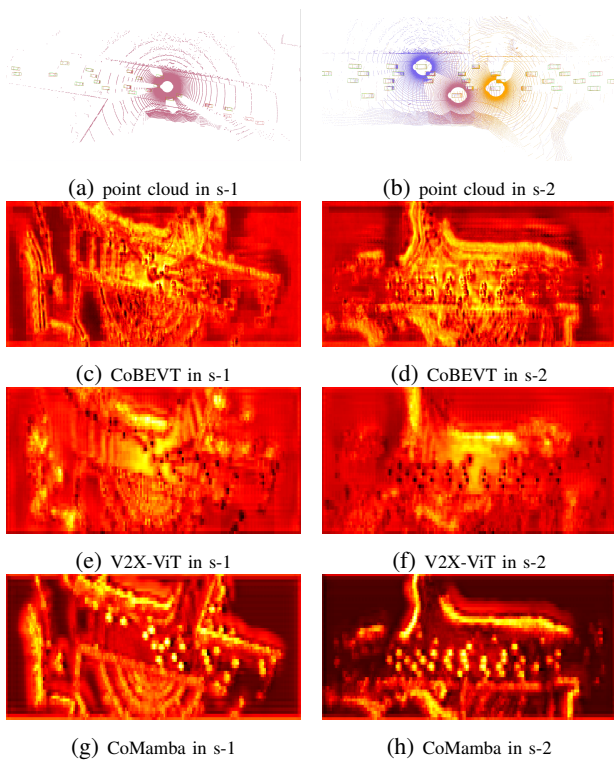


Fig. 5: **Visualization of Fused Intermediate Features on the OPV2V Default Testing Set.** We compared the fused intermediate features from our method, CoMamba, against other SOTA methods, V2X-ViT and CoBEVT, using two samples. The first row shows two point cloud samples from our CoMamba, corresponding to the fused intermediate features in the following rows. It is evident that our fused intermediate features are clearer, with more accurate local features corresponding to objects. Additionally, the shape of the scenario modeling is more complete compared to the other methods.

Even when the number of agents increases to 10, CoMamba maintains a solid performance with 7.6 FPS and a GPU memory usage of 7.3 GB. The linear time complexity of our CoMamba makes it particularly advantageous for real-time 3D perception in real-world, large-scale driving scenarios.

Visualization. Fig. 4 presents 3D detection visualization ex-

amples from V2X-ViT [5], CoBEVT [2], and our CoMamba across three testing sets. It is evident that our proposed CoMamba achieves more accurate 3D detection results in both simulated and real-world point cloud scenarios, demonstrating its superior performance in cooperative perception tasks. We visually present intermediate features in Fig. 5 using two point cloud samples.

Ablation study. Table III highlights the significance of our proposed CSS2D and GPM within the CoMamba framework on the V2XSet [5] and V2V4Real [19] testing sets. The baseline is a simple averaging fusion method with a 1×1 convolution layer. Integrating CSS2D and GPM into CoMamba resulted in performance improvements of 15.4%/11.4% for AP@0.5/0.7 compared to the Baseline on the V2V4real testing set, underscoring their substantial contribution to the overall performance.

V. CONCLUSION

In this paper, we introduce a novel attention-free, state space model-based framework called CoMamba for V2X-based perception. Our innovative framework incorporates two major components: the Cooperative 2D-Selective-Scan Module (CSS2D) and the Global-wise Pooling Module (GPM), which are responsible for enhancing global interaction efficiently and could be utilized in future large-scale V2X perception scenarios. By leveraging the advantages of SSMS, CoMamba enables real-time cooperative perception with an impressive inference speed of 26.9 FPS while utilizing only 0.64 GB of GPU memory footprint. Furthermore, CoMamba scales remarkably well, achieving linear-complexity costs in GFLOPs, latency, and GPU memory relative to the number of agents, while still maintaining excellent perception performance. Our extensive experiments on both simulated and real-world V2X datasets demonstrate that CoMamba surpasses other state-of-the-art cooperative perception methods on the 3D point cloud object detection task. We envision that our work will facilitate novel architectural designs and practical onboard solutions for real-time cooperative autonomy.

REFERENCES

- [1] R. Xu, H. Xiang, X. Xia, X. Han, J. Li, and J. Ma, "Opv2v: An open benchmark dataset and fusion pipeline for perception with vehicle-to-vehicle communication," in *2022 International Conference on Robotics and Automation (ICRA)*. IEEE, 2022, pp. 2583–2589.
- [2] R. Xu, Z. Tu, H. Xiang, W. Shao, B. Zhou, and J. Ma, "Cobevt: Cooperative bird's eye view semantic segmentation with sparse transformers," *arXiv preprint arXiv:2207.02202*, 2022.
- [3] Q. Chen, X. Ma, S. Tang, J. Guo, Q. Yang, and S. Fu, "F-cooper: Feature based cooperative perception for autonomous vehicle edge computing system using 3d point clouds," in *Proceedings of the 4th ACM/IEEE Symposium on Edge Computing*, 2019, pp. 88–100.
- [4] A. Dosovitskiy, L. Beyer, A. Kolesnikov, D. Weissenborn, X. Zhai, T. Unterthiner, M. Dehghani, M. Minderer, G. Heigold, S. Gelly *et al.*, "An image is worth 16x16 words: Transformers for image recognition at scale," *arXiv preprint arXiv:2010.11929*, 2020.
- [5] R. Xu, H. Xiang, Z. Tu, X. Xia, M.-H. Yang, and J. Ma, "V2x-vit: Vehicle-to-everything cooperative perception with vision transformer," in *European conference on computer vision*. Springer, 2022, pp. 107–124.
- [6] J. Li, R. Xu, X. Liu, B. Li, Q. Zou, J. Ma, and H. Yu, "S2r-vit for multi-agent cooperative perception: Bridging the gap from simulation to reality," *arXiv preprint arXiv:2307.07935*, 2023.
- [7] H. Xiang, R. Xu, and J. Ma, "Hm-vit: Hetero-modal vehicle-to-vehicle cooperative perception with vision transformer," in *Proceedings of the IEEE/CVF International Conference on Computer Vision*, 2023, pp. 284–295.
- [8] A. Gu, K. Goel, and C. Ré, "Efficiently modeling long sequences with structured state spaces," *arXiv preprint arXiv:2111.00396*, 2021.
- [9] T. Dao, D. Y. Fu, K. K. Saab, A. W. Thomas, A. Rudra, and C. Ré, "Hungry hungry hippos: Towards language modeling with state space models," in *Proceedings of the 11th International Conference on Learning Representations (ICLR)*, 2023.
- [10] J. T. Smith, A. Warrington, and S. W. Linderman, "Simplified state space layers for sequence modeling," *arXiv preprint arXiv:2208.04933*, 2022.
- [11] A. Gu and T. Dao, "Mamba: Linear-time sequence modeling with selective state spaces," *arXiv preprint arXiv:2312.00752*, 2023.
- [12] H. Zhao, M. Zhang, W. Zhao, P. Ding, S. Huang, and D. Wang, "Cobra: Extending mamba to multi-modal large language model for efficient inference," *arXiv preprint arXiv:2403.14520*, 2024.
- [13] Y. Qiao, Z. Yu, L. Guo, S. Chen, Z. Zhao, M. Sun, Q. Wu, and J. Liu, "Vl-mamba: Exploring state space models for multimodal learning," *arXiv preprint arXiv:2403.13600*, 2024.
- [14] W. Li, X. Hong, and X. Fan, "Spikemba: Multi-modal spiking saliency mamba for temporal video grounding," *arXiv preprint arXiv:2404.01174*, 2024.
- [15] J. Ma, F. Li, and B. Wang, "U-mamba: Enhancing long-range dependency for biomedical image segmentation," *arXiv preprint arXiv:2401.04722*, 2024.
- [16] T. Huang, X. Pei, S. You, F. Wang, C. Qian, and C. Xu, "Localmamba: Visual state space model with windowed selective scan," *arXiv preprint arXiv:2403.09338*, 2024.
- [17] J. Liu, H. Yang, H.-Y. Zhou, Y. Xi, L. Yu, Y. Yu, Y. Liang, G. Shi, S. Zhang, H. Zheng *et al.*, "Swin-umamba: Mamba-based unet with imagenet-based pretraining," *arXiv preprint arXiv:2402.03302*, 2024.
- [18] S. Yang, Y. Wang, and H. Chen, "Mambamil: Enhancing long sequence modeling with sequence reordering in computational pathology," *arXiv preprint arXiv:2403.06800*, 2024.
- [19] R. Xu, X. Xia, J. Li, H. Li, S. Zhang, Z. Tu, Z. Meng, H. Xiang, X. Dong, R. Song *et al.*, "V2v4real: A real-world large-scale dataset for vehicle-to-vehicle cooperative perception," in *Proceedings of the IEEE/CVF Conference on Computer Vision and Pattern Recognition*, 2023, pp. 13 712–13 722.
- [20] Y. Lu, Q. Li, B. Liu, M. Dianati, C. Feng, S. Chen, and Y. Wang, "Robust collaborative 3d object detection in presence of pose errors," in *2023 IEEE International Conference on Robotics and Automation (ICRA)*. IEEE, 2023, pp. 4812–4818.
- [21] Z. Meng, X. Xia, R. Xu, W. Liu, and J. Ma, "Hydro-3d: Hybrid object detection and tracking for cooperative perception using 3d lidar," *IEEE Transactions on Intelligent Vehicles*, 2023.
- [22] Y.-C. Liu, J. Tian, N. Glaser, and Z. Kira, "When2com: Multi-agent perception via communication graph grouping," in *Proceedings of the IEEE/CVF Conference on computer vision and pattern recognition*, 2020, pp. 4106–4115.
- [23] Y. Li, S. Ren, P. Wu, S. Chen, C. Feng, and W. Zhang, "Learning distilled collaboration graph for multi-agent perception," *Advances in Neural Information Processing Systems*, vol. 34, pp. 29 541–29 552, 2021.
- [24] Y. Hu, S. Fang, Z. Lei, Y. Zhong, and S. Chen, "Where2comm: Communication-efficient collaborative perception via spatial confidence maps," *Advances in neural information processing systems*, vol. 35, pp. 4874–4886, 2022.
- [25] K. Yang, D. Yang, J. Zhang, M. Li, Y. Liu, J. Liu, H. Wang, P. Sun, and L. Song, "Spatio-temporal domain awareness for multi-agent collaborative perception," in *Proceedings of the IEEE/CVF International Conference on Computer Vision*, 2023, pp. 23 383–23 392.
- [26] R. Xu, W. Chen, H. Xiang, X. Xia, L. Liu, and J. Ma, "Model-agnostic multi-agent perception framework," in *2023 IEEE International Conference on Robotics and Automation (ICRA)*. IEEE, 2023, pp. 1471–1478.
- [27] R. Xu, J. Li, X. Dong, H. Yu, and J. Ma, "Bridging the domain gap for multi-agent perception," in *2023 IEEE International Conference on Robotics and Automation (ICRA)*. IEEE, 2023, pp. 6035–6042.
- [28] J. Li, R. Xu, X. Liu, J. Ma, Z. Chi, J. Ma, and H. Yu, "Learning for vehicle-to-vehicle cooperative perception under lossy communication," *IEEE Transactions on Intelligent Vehicles*, 2023.
- [29] S. Ren, Z. Lei, Z. Wang, M. Dianati, Y. Wang, S. Chen, and W. Zhang, "Interruption-aware cooperative perception for v2x communication-aided autonomous driving," *IEEE Transactions on Intelligent Vehicles*, 2024.
- [30] J. Li, B. Li, X. Liu, J. Fang, F. Juefei-Xu, Q. Guo, and H. Yu, "Advgps: Adversarial gps for multi-agent perception attack," in *IEEE International Conference on Robotics and Automation*, 2024.
- [31] Y. Li, Q. Fang, J. Bai, S. Chen, F. Juefei-Xu, and C. Feng, "Among us: Adversarially robust collaborative perception by consensus," in *Proceedings of the IEEE/CVF International Conference on Computer Vision*, 2023, pp. 186–195.
- [32] Z. Song, F. Wen, H. Zhang, and J. Li, "A cooperative perception system robust to localization errors," in *2023 IEEE Intelligent Vehicles Symposium (IV)*. IEEE, 2023, pp. 1–6.
- [33] M. A. Khan, S. Ghosh, S. A. Busari, K. M. S. Huq, T. Dagiuklas, S. Mumtaz, M. Iqbal, and J. Rodriguez, "Robust, resilient and reliable architecture for v2x communications," *IEEE Transactions on Intelligent Transportation Systems*, vol. 22, no. 7, pp. 4414–4430, 2021.
- [34] J. Li, B. Li, X. Liu, R. Xu, J. Ma, and H. Yu, "Breaking data silos: Cross-domain learning for multi-agent perception from independent private sources," in *IEEE International Conference on Robotics and Automation*, 2024.
- [35] J. Li, R. Xu, X. Liu, B. Li, Q. Zou, J. Ma, and H. Yu, "S2r-vit for multi-agent cooperative perception: Bridging the gap from simulation to reality," in *IEEE International Conference on Robotics and Automation*, 2024.
- [36] L. Zhu, B. Liao, Q. Zhang, X. Wang, W. Liu, and X. Wang, "Vision mamba: Efficient visual representation learning with bidirectional state space model," *arXiv preprint arXiv:2401.09417*, 2024.
- [37] Y. Liu, Y. Tian, Y. Zhao, H. Yu, L. Xie, Y. Wang, Q. Ye, and Y. Liu, "Vmamba: Visual state space model," *arXiv preprint arXiv:2401.10166*, 2024.
- [38] A. Gu, I. Johnson, K. Goel, K. Saab, T. Dao, A. Rudra, and C. Ré, "Combining recurrent, convolutional, and continuous-time models with linear state space layers," *Advances in neural information processing systems*, vol. 34, pp. 572–585, 2021.
- [39] T.-Y. Lin, P. Goyal, R. Girshick, K. He, and P. Dollár, "Focal loss for dense object detection," in *IEEE International Conference on Computer Vision*, 2017, pp. 2980–2988.
- [40] R. Xu, Y. Guo, X. Han, X. Xia, H. Xiang, and J. Ma, "Openeda: an open cooperative driving automation framework integrated with co-simulation," in *2021 IEEE International Intelligent Transportation Systems Conference (ITSC)*. IEEE, 2021, pp. 1155–1162.
- [41] T.-H. Wang, S. Manivasagam, M. Liang, B. Yang, W. Zeng, and R. Urtasun, "V2vnet: Vehicle-to-vehicle communication for joint perception and prediction," in *Computer Vision—ECCV 2020: 16th European Conference, Glasgow, UK, August 23–28, 2020, Proceedings, Part II 16*. Springer, 2020, pp. 605–621.
- [42] A. H. Lang, S. Vora, H. Caesar, L. Zhou, J. Yang, and O. Beijbom, "Pointpillars: Fast encoders for object detection from point clouds," in *Proceedings of the IEEE/CVF conference on computer vision and pattern recognition*, 2019, pp. 12 697–12 705.

- [43] I. Loshchilov and F. Hutter, “Decoupled weight decay regularization,” *arXiv preprint arXiv:1711.05101*, 2017.